Light refraction in the Earth's atmosphere IV. The rainbow

A. Cesanelli

Centro de Investigaciones Geofísicas (CIGEOF)
Facultad de Ciencias Astronómicas y Geofísicas, Universidad Nacional de La Plata (FCAG, UNLP),
Paseo del Bosque s/n, La Plata, Buenos Aires, Argentina; TE: (54) 221 4236593. Fax: (54) 221 4236591.
https://orcid.org/0009-0006-9896-7499
e-mail: acesanelli@fcaglp.unlp.edu.ar

A. Cruzado

Facultad de Ciencias Astronómicas y Geofísicas, Universidad Nacional de La Plata (FCAG, UNLP),
Paseo del Bosque s/n, La Plata, Buenos Aires, Argentina; TE: (54) 221 4236593. Fax: (54) 221 4236591.
Instituto de Astrofísica de La Plata (IALP, CONICET), Paseo del Bosque s/n, 1900 La Plata, Buenos Aires, Argentina
https://orcid.org/0000-0001-5936-195X
e-mail: acruzado@fcaglp.unlp.edu.ar; alicehaiadjamian@yahoo.com.ar

C. A. Paola

Facultad de Ciencias Astronómicas y Geofísicas, Universidad Nacional de La Plata (FCAG, UNLP),
Paseo del Bosque s/n, La Plata, Buenos Aires, Argentina; TE: (54) 221 4236593. Fax: (54) 221 4236591.
Universidad Tecnológica Nacional, Facultad Regional La Plata (UTN, FRLP),
Avenida 60 esquina 124 s/n, La Plata, Buenos Aires, Argentina; Tel: (54) 221 4124300.
https://orcid.org/0009-0005-6580-3327
e-mail: apaola@fcaglp.unlp.edu.ar

Received 2 September 2025; accepted 13 November 2025

We approach the study of the rainbow with two primary objectives: 1) to analyze the explicit dependence of the intensity and angular position of the first-order rainbow on different parameters, critically, water temperature; 2) to compare the results of geometric optics with those derived from wave theory. To achieve this, we implemented a discretization method to circumvent the obstacle posed by geometric optics, where the cross-section, and thus light intensity, diverges at the minimum deviation angle. Wave phenomena were incorporated using the Airy approximation. Through calculations spanning a broad range of parameter values, we derived analytical expressions that efficiently compute both the light intensity at the first-order rainbow's peak and its angular position, as functions of light wavelength, drop radius, and water temperature.

Keywords: Planetary atmospheres; light refraction; rainbow.

DOI: https://doi.org/10.31349/RevMexFis.72.031301

1. Introduction

This article is the fourth in a series we have titled *Light refraction in the Earth's atmosphere*, through which we aim to advance the understanding of optical phenomena occurring in the terrestrial atmosphere. Both inferior mirages, the focus of our previous articles [1–3], and rainbows, the subject of this work, involve refraction processes. In mirages, sunlight refracts as it passes through atmospheric layers with varying refractive indices. In rainbows, refraction occurs at the air-water interface. These and other atmospheric optical phenomena have been of great interest to many researchers, with a multitude of articles published over time. Although their fundamental nature is well understood, increasingly efficient computational tools continue to emerge. Using these advances, we can now explore previously unexamined aspects of these phenomena.

The rainbow, in particular, is a phenomenon for which humans have sought rational explanations since Aristotle's time. Beginning with Descartes, who first concluded that rainbows are formed by sunlight emerging from raindrops after penetrating and reflecting internally, and Newton, who explained the colors of the rainbow by accounting for the wavelength-dependent refractive index of water, the phenomenon has been analyzed through various theoretical frameworks and at varying depths. The foundational works of Young [4] and Airy [5] introduced wave phenomena within a semiclassical approximation, while Mie [6] provided an exact theory based on Maxwell's equations. Modern contributions such as those by Nussenzveig [7–9], Walker [10], Mobbs [11] and Casini & Covello [12] represent just a few of countless published studies. Extensive reviews and books on rainbows and related optical phenomena *e.g.*, [13–15] further enrich this corpus.

Although the physics of the rainbow has been studied for centuries, over recent decades the observation of this natural phenomenon has been transformed into a powerful diagnostic technique for engineering and science. In this way,

theoretical findings have paved the way for techniques that allow inferring the physical properties of liquid droplets and thus characterize sprays created in different scenarios (fuel injection in internal combustion engines, agricultural spraying systems, cooling towers, atmospheric studies, etc.) by examining the rainbow patterns they generate. In particular, rainbow refractometry has established itself as a benchmark non-intrusive optical technique for droplet characterization. The foundations of this methodology, initially introduced by Roth and colleagues [16, 17], were further developed by Van Beeck and Riethmuller [18], who demonstrated the feasibility of simultaneously determining the size and refractive index of spherical droplets by analyzing the rainbow pattern. This is achieved by exploiting the dependence of the interference fringe spacing on droplet diameter, and the angular position of the rainbow peak on the refractive index, and, consequently, on temperature. This principle was expanded and consolidated in the doctoral thesis of Van Beeck [19], which integrated velocity measurement, thereby developing a triple-diagnostic technique: size, temperature, and velocity. His work also provides a detailed analysis of scattering patterns for both spherical and non-spherical droplets, proposing experimental and theoretical improvements that strengthen the applicability of the method to real sprays.

Rainbow refractometry became a standard for spray characterization not only of water but also of other liquids and in different scenarios. Using the global rainbow technique, Saengkaew [20], for example, determined the droplet temperature and size distribution of a biodiesel spray under ambient and combustion conditions. Also, Chanisa [21], using global rainbow refractometry, carried out refractive index measurements on free-falling water and ethanol droplets under high pressure. The field has evolved towards addressing more complex scenarios, such as non-isothermal droplets. In this context, Lv *et al.* [22] investigated the surface temperature of oscillating droplets through surface tension measurements. These surface temperatures were then compared to those volume-averaged obtained via rainbow refractometry, in order to assess the accuracy and applicability of the rainbow technique under dynamic heating and cooling conditions.

While rainbows have been the subject of extensive theoretical and applied research, this and future work aim to explore previously overlooked aspects. One such aspect is their specific dependence on atmospheric conditions which, in turn, determine the characteristics of the water drops responsible for rainbow formation.

In this article, we begin by examining the dependence of rainbow appearance on drop size and water temperature. Although it is well known that larger drops result in sharper rainbows, we approach the subject with the aim of analyzing the specific mathematical dependence of the rainbow light intensity and the so-called rainbow angle on drop size. With the same goal, we investigate the influence of water temperature on the appearance of the rainbow, which can be done by considering the dependence of the refractive index of water on this parameter. As water is the most abundant liquid on Earth, the behavior of its refractive index with temperature has gained increasing interest, particularly for industrial and biophysical applications. Several studies [23, 24] have addressed this topic and we build on their findings here.

In this article, it is also of interest to compare results obtained within the framework of geometric optics with those obtained by considering wave phenomena. When working within the framework of geometric optics, we encounter a serious hurdle if the so-called Descartes ray is involved. As is well known, this theory predicts an infinite light intensity for the minimum deviation angle. In order to overcome this obstacle, we propose a possible solution by discretizing a differential problem.

We organize this article as follows. In Sec. 2, we present the analysis of the rainbow from the perspective of geometric optics, separating the treatment into five subsections. In the first subsection, we discuss the geometric aspect of the rainbow, revisiting well-known results that nevertheless need to be reproduced here. Besides providing a suitable context for nonspecialist readers, we require explicit expressions, written in our own notation, that we use for our calculations in further sections. In the second subsection, following the same logic, we examine the energy aspect of the phenomenon by defining transmittance and reflectance in terms of Fresnel coefficients. In the third subsection, we address the problem of calculating the differential cross-section, tending to infinity near the Descartes ray. Then, in the fourth subsection, we propose a possible way to overcome this hurdle that arises within the framework of geometric optics. Finally, in the fifth subsection we present expressions that arise from the dependence of water refractive index on the wavelength of light and the temperature of water. In Sec. 3, we present the expressions we use to calculate the luminous intensity of the rainbow as a function of different variables within the framework of Airy's theory, while also justifying our choice of this semi-classical theory over others. Then, in Sec. 4, we present and discuss our results, obtained within the framework of geometric optics and Airy's theory. Finally, in Sec. 5 we provide a brief summary and present our conclusions.

2. Treatment of the rainbow within the framework of geometric optics

2.1. Geometry and basic physics of the rainbow

Figure 1 depicts the widely known geometry of the ray path that gives rise to the rainbow. It shows a light ray striking a spherical water drop forming an angle α with the radial direction and its subsequent trajectory inside the drop (which forms an angle β with the radial direction) after two successive internal reflections. Denoting the refractive index of the water by n and considering the refractive index of air to be equal to 1, by successively applying Snell's law (*i.e.* $\sin\alpha = n\sin\beta$) it can be shown that all internal angles β

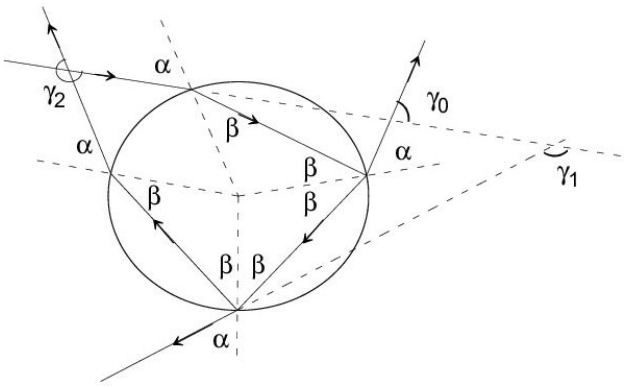

FIGURE 1. Rainbow formation geometry. The diagram depicts an incident light ray striking a water drop and three resulting emergent rays corresponding to 0, 1, and 2 internal reflections.

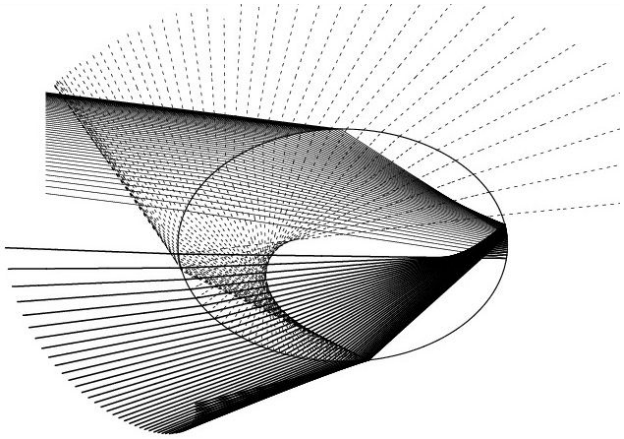

FIGURE 2. Families of incident and emergent rays. Thin solid lines represent a family of incident rays on a water drop, thick solid lines show a family of emergent rays forming the first-order rainbow, and dashed lines depict a family of emergent rays forming the second-order rainbow.

are equal to each other, and all external angles α are equal to each other.

The figure also displays emergent rays from the drop corresponding to the transmitted portion of light, one of them exiting through the back of the drop, another contributing to the first-order rainbow, and the third contributing to the second-order rainbow. By also applying Snell's law, an expression can be found for the angle that each emerging ray makes with the original direction of the incident ray:

$$\gamma_m = 2\,(\alpha - \beta) + m\,(\pi - 2\beta)\,, \tag{1}$$

where m represents the number of internal reflections undergone by the ray before emerging from the drop. Following this notation, $m = 0$ corresponds to the light emerging from the back of the drop (not visible to the observer), $m = 1$ to the emergent light forming the first-order rainbow, $m = 2$ describes the emergent light forming the second-order rainbow, etc. Writing β as a function of α from Snell's law, Eq. (1) can be expressed as follows:

$$\gamma_m = 2\alpha - 2(m+1)\arcsin\left(\frac{\sin\alpha}{n}\right) + m\pi. \tag{2}$$

By repeating the ray tracing procedure for different incident angles we obtain a family of emerging rays that give rise to each m-order rainbow. For example, in Fig. 2 we represent the families of rays that form the first- and second-order rainbows. From this figure it becomes evident the existence of minimum deviation angles which, in fact, make the existence of rainbows possible. These relative extremum in the interval $0^\circ \leq \alpha \leq 90^\circ$ for $m > 0$ can also be observed in Fig. 3, where γ as a function of α is plotted for $m = 1$ and $m = 2$. Since in this section we only intend to show the general behavior of γ as a function of α for different values of m, this figure was constructed for a refractive index value of $n = 1.33$, commonly adopted for water.

In order to calculate the relative extremum angles, we differentiate Eq. (2) with respect to α, which gives:

$$\frac{d\gamma_m}{d\alpha} = 2 - \frac{2\,(m+1)\cos\alpha}{n\sqrt{1 - \frac{\sin^2\alpha}{n^2}}}. \tag{3}$$

Equating Eq. (3) to zero we obtain the following expressions for $\alpha_{m,MC}$, values of α for which the relative extrema of γ_m occur:

$$\cos\alpha_{m,MC} = \sqrt{\frac{n^2-1}{m\,(m+2)}},$$
$$\sin\alpha_{m,MC} = \sqrt{\frac{(m+1)^2 - n^2}{(m+1)^2 - 1}}. \tag{4}$$

In these expressions and henceforth, the subscript MC stands for *Maximum*, referring to all aspects related to the intensity peak, and *Classical*, referring to classical physics within the framework in which we work. It can also be verified that the relative extrema occurring in $\alpha_{m,MC}$ are, in fact, the minima of the function given by Eq. (2). Thus, replacing α with $\alpha_{m,MC}$ given by Eq. (4), the minimum deviation angle, $\gamma_{m,MC}$ is obtained:

$$\gamma_{m,MC} = m\pi + 2\arcsin\left[\sqrt{\frac{(m+1)^2 - n^2}{(m+1)^2 - 1}}\right]$$
$$- 2\,(m+1)\arcsin\left[\frac{1}{n}\sqrt{\frac{(m+1)^2 - n^2}{(m+1)^2 - 1}}\right]. \tag{5}$$

From these expressions and also from Fig. 3 it is verified that $\alpha_{m,MC}$ increases as m increases, whereas for $m = 0$, it is instead an increasing function of α throughout the interval.

2.2. Energetic aspects of the rainbow

To calculate the fraction of light intensity leaving the drop relative to the incident light, we must use the Fresnel coefficients, which represent ratios between the amplitudes of reflected and incident, or transmitted and incident, electric

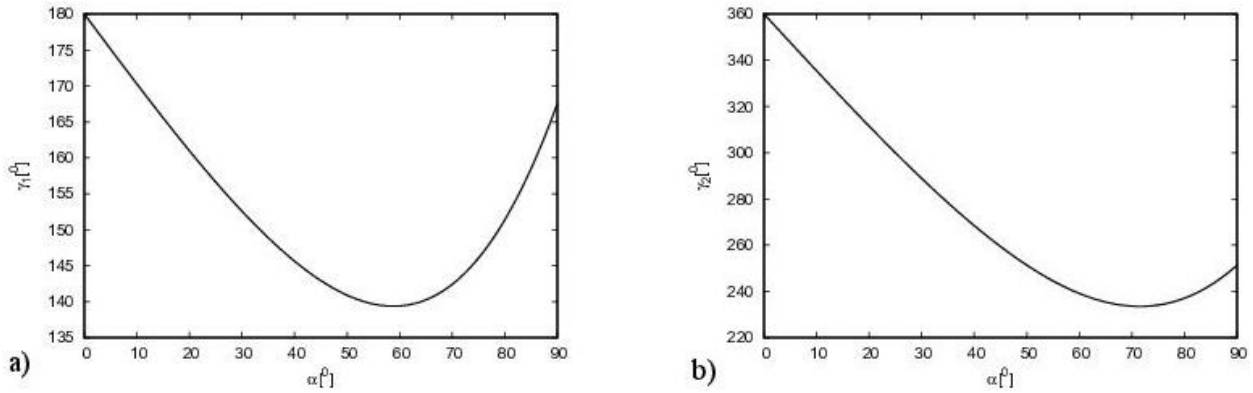

FIGURE 3. a) The exit angle γ as a function of the entrance angle α is shown for a single internal reflection in a water drop and b) two internal reflections.

waves (indicated as E_{oi}, E_{or} and E_{ot}), vibrating parallel or transverse to the incidence plane (indicated with symbols $\parallel$ and $\perp$, respectively). Being n_i and n_t the refractive indices of the incident and transmitted media, and θ_i and θ_t the angles of incidence and transmission, respectively, the Fresnel coefficients are expressed as:

$$r_{\parallel} = \left(\frac{E_{0r}}{E_{0i}}\right)_{\parallel} = \frac{n_t\ \cos\theta_i - n_i \cos\theta_t}{n_t\ \cos\theta_i + n_i \cos\theta_t}, \tag{6}$$

$$t_{\parallel} = \left(\frac{E_{0t}}{E_{0i}}\right)_{\parallel} = \frac{2\ n_i \cos\theta_i}{n_t\ \cos\theta_i + n_i \cos\theta_t}, \tag{7}$$

$$r_{\perp} = \left(\frac{E_{0r}}{E_{0i}}\right)_{\perp} = \frac{n_i \cos\theta_i - n_t\ \cos\theta_t}{n_i \cos\theta_i + n_t\ \cos\theta_t}, \tag{8}$$

$$t_{\perp} = \left(\frac{E_{0t}}{E_{0i}}\right)_{\perp} = \frac{2\ n_i \cos\theta_i}{n_i \cos\theta_i + n_t\ \cos\theta_t}. \tag{9}$$

It is in terms of these coefficients that the reflectance $(R_{\parallel}, R_{\perp})$ and transmittance $(T_{\parallel}, T_{\perp})$ are subsequently expressed, representing the fraction of incident light, whether vibrating paralel or perpendicular to the incidence plane, that is reflected or transmitted, respectively, at each interface. We can then write:

$$R_{\parallel,\perp} = \left(\frac{E_{0r}}{E_{0i}}\right)^2_{\parallel,\perp} = (r)^2_{\parallel,\perp}\,,$$

$$T_{\parallel,\perp} = \frac{n_t\ \cos\theta_t}{n_i \cos\theta_i}\left(\frac{E_{0t}}{E_{0i}}\right)^2_{\parallel,\perp} = \frac{n_t\ \cos\theta_t}{n_i \cos\theta_i}\,(t)^2_{\parallel,\perp}\,. \tag{10}$$

Taking into account the number of internal reflections occurring before the light leaves the drop, and further considering that all angles inside the drop are equal to β and that both the original angle of incidence of sunlight on the drop and all exit angles from it are equal to α, the fractions of outgoing light, vibrating parallel or perpendicular to the incidence plane, relative to the initially incident light after m internal reflections can be written as:

$$T_{\parallel} = \left(1 - R_{\parallel}\right)^2 R^m_{\parallel} = \left(1 - \left(\frac{n\cos\alpha - \cos\beta}{n\cos\alpha + \cos\beta}\right)^2\right)^2 \times \left(\frac{n\cos\alpha - \cos\beta}{n\cos\alpha + \cos\beta}\right)^{2m},$$

$$T_{\perp} = \left(1 - R_{\perp}\right)^2 R^m_{\perp} = \left(1 - \left(\frac{\cos\alpha - n\ \cos\beta}{\cos\alpha + n\ \cos\beta}\right)^2\right)^2 \times \left(\frac{\cos\alpha - n\ \cos\beta}{\cos\alpha + n\ \cos\beta}\right)^{2m}. \tag{11}$$

2.3. Cross-section

Let $\mathcal{I}_0$ be the incident light per unit area and time in direction r_α, forming an angle α with the radial direction, and $J(\gamma)$ the transmitted light per unit solid angle and time in direction r_γ, forming an angle γ with the incident beam direction. Our objective is to determine $J(\gamma)/\mathcal{I}_0$, known as the cross-section, which can be approached as a problem of particles scattered by a central potential. In this framework, $\mathcal{I}_0$ can be interpreted as the number of particles crossing any area element perpendicular to the incident sunlight beam per unit area and unit time. $J(\gamma)$ is then interpreted as the number of particles scattered in a direction r_γ per unit solid angle and unit time. Calculating $J(\gamma)$ requires finding the particle deflection angle as a function of the impact parameter b, denoted $\gamma(b)$. This angle is precisely the one indicated in Fig. 1 and represents the angle that the direction of scattered particles makes with the direction of incident particles. In Fig. 2 the impact parameter b is represented for a light ray incident at angle α on a water drop of radius R.

A ring-shaped area element dA on the drop surface can be characterized by its impact parameter b and width db. The area of the ring can then be written as:

$$dA = 2\pi\ b(\gamma)\ db(\gamma). \tag{12}$$

The number of incident particles passing through the area element dA per unit time is then:

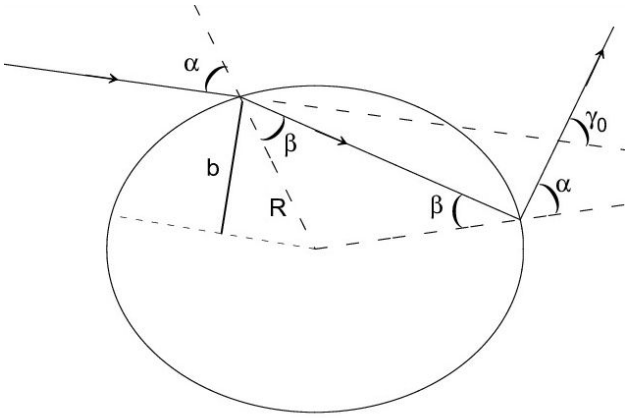

FIGURE 4. The impact parameter, b, is derived from the geometric relationship with the drop radius, R, and the angle, α, formed between the incident ray and the radial direction.

$$dN_i = \mathcal{I}_0\, dA = 2\pi\, b(\gamma)\, \mathcal{I}_0\, db(\gamma). \tag{13}$$

If for that impact parameter the particles are scattered in the direction r_γ, the particles that passed through the area element dA in the time interval dt after being scattered will pass through the area element dA' that subtends the solid angle $d\Omega$. This last area element can be written as:

$$dA' = R^2 d\Omega = 2\pi R^2\, \sin\gamma\, d\gamma. \tag{14}$$

The number of particles scattered through the area element dA' per unit of time is then:

$$dN_d = J(\gamma)\, d\Omega = J(\gamma)\, 2\pi\, \sin\gamma\, d\gamma. \tag{15}$$

Since the number of scattered particles that pass through the area element dA' per unit of time must be equal to the number of incident particles on dA per unit of time (assuming there are no losses along the way, which in the case of the rainbow are taken later into account in the transmittance), it is true that:

$$J(\gamma)\, 2\pi\, \sin\gamma\, d\gamma = 2\pi\, b(\gamma)\, \mathcal{I}_0\, db(\gamma). \tag{16}$$

Then,

$$\frac{J(\gamma)}{\mathcal{I}_0} = \frac{b(\gamma)}{\sin\gamma}\frac{db(\gamma)}{d\gamma}. \tag{17}$$

The relation $J(\gamma)/\mathcal{I}_0$ is usually called the differential scattering cross-section and is often expressed as

$$\frac{J(\gamma)}{\mathcal{I}_0} = \frac{d\sigma(\gamma)}{d\Omega}, \tag{18}$$

hence being

$$\frac{d\sigma(\gamma)}{d\Omega} = \frac{b(\gamma)}{\sin\gamma}\frac{db(\gamma)}{d\gamma}. \tag{19}$$

Note that, while $\mathcal{I}_0$ represents the energy per unit time and unit area, $J(\gamma)$ is the energy per unit time and unit solid angle. The left-hand side of Eq. (18) then has units of area, such as the cross-section on the right-hand side.

To calculate the cross-section we take into account that $b = R\, \sin\alpha$ (see Fig. 4), and therefore

$$\frac{db(\gamma)}{d\gamma} = R\cos\alpha\, \frac{d\alpha}{d\gamma}. \tag{20}$$

Taking into account that $d\alpha/d\gamma$ is the inverse of the derivative given by Eq. (3), and that this reasoning is valid for any number m of internal reflections, it follows that:

$$\left.\frac{db(\gamma)}{d\gamma}\right|_m = \frac{R\cos\alpha\, \sqrt{n^2-\sin^2\alpha}}{2\,\sqrt{n^2-\sin^2\alpha} - 2\,(m+1)\cos\alpha}. \tag{21}$$

By substituting this last expression and the expression for γ given by Eq. (2) into Eq. (19), we could then obtain the desired cross-section. However, it is clear that such a cross-section tends to infinity at the minimum deviation angle. Since $\alpha_{m,MC}$ is a minimum of the function $\gamma(\alpha)$, $d\alpha/d\gamma|_m$, and consequently $db(\gamma)/d\gamma$, tend to infinity at the minimum deviation angle. Therefore,

$$\gamma \to \gamma_{m,MC} \implies \left.\frac{d\sigma(\gamma)}{d\Omega}\right|_m \to \infty.$$

2.4. Calculation methodology

As we mentioned before, within the framework of geometric optics it is not possible to use differential cross sections near the minimum-deviation angle. In order to overcome this limitation in the analysis, we propose to discretize the problem. Thus, we consider the outgoing light energy not for individual values of γ but rather within different intervals of γ values. From Eq. (18) we can write:

$$\mathcal{I}_0\, d\sigma(\gamma) = J(\gamma)\, d\Omega, \tag{22}$$

where $d\sigma(\gamma)$ can be interpreted as the differential area through which, in a given time, passes a number of incident beam particles equal to the number of scattered beam particles passing through the differential solid angle $d\Omega$. Following the reasoning outlined in the previous section we can now say, by discretizing the problem, that the light energy entering the drop through a ring of area

$$\Delta\sigma(\gamma) = 2\pi\, b(\gamma)\Delta b = 2\pi R^2 \sin\alpha\cos\alpha\Delta\alpha, \tag{23}$$

emerges from it within the solid angle of half-angle $\Delta\gamma$ given by

$$\Delta\Omega = 2\pi \sin\gamma\Delta\gamma, \tag{24}$$

where $\Delta\alpha$ is the interval of α values that contribute to the assumed interval $\Delta\gamma$. That is, any ray entering the drop at an angle α relative to the radial direction within the $\Delta\alpha$ interval will emerge in a direction that forms an angle γ with the

initial direction within the $\Delta\gamma$ interval. The outgoing light energy within this $\Delta\Omega$ solid angle of half-angle $\Delta\gamma$ is then given by:

$$J(\gamma)2\pi\sin\gamma\Delta\gamma = \mathcal{I}_0\ 2\pi R^2\sin\alpha\cos\alpha\Delta\alpha. \tag{25}$$

Taking into account the losses from successive reflections and transmissions, the outgoing light intensity, $I(\gamma)$, is written as:

$$I(\gamma) = \mathcal{I}_0 R^2\ \frac{\sin\alpha\cos\alpha}{\sin\gamma}\ \frac{\Delta\alpha}{\Delta\gamma}\ (T_\perp + T_\parallel), \tag{26}$$

where $T_\perp$ and $T_\parallel$ are given by Eqs. (11).

To perform our calculations, we proceed specifically as follows. First, we set an interval $\Delta\gamma$. Then we divide the full range of values that γ takes for $0^\circ \leq \alpha \leq 90^\circ$, from $\gamma_{m,MC}$ up to its maximum value (180° if $m = 1$), into equal subintervals of size $\Delta\gamma$. Next, for each of these subintervals, all of equal width $\Delta\gamma$ but centered at different γ values, we compute the corresponding $\Delta\alpha$ interval(s) of α values that contribute to the given $\Delta\gamma$. This requires numerically solving Eq. (2). Note that the intervals $\Delta\alpha$ are not only centered on different values of α, but are also, unlike $\Delta\gamma$, all distinct. Moreover, since $\gamma(\alpha)$ is not a single-valued function over the entire range $0^\circ \leq \alpha \leq 90^\circ$ (see Fig. 3), most of the $\Delta\gamma$ intervals are mapped to two $\Delta\alpha$ intervals each. Finally, we compute $T_\perp$ and $T_\parallel$ using Eqs. (11) to determine the intensity of the light via 26. In this procedure, the key issue is how to select an appropriate $\Delta\gamma$ interval.

2.5. Refractive index of water

To account for the effect of both light wavelength and water temperature in the analysis, we propose to calculate the refractive index using the expression derived by Bashkatov A. N. and Genina E. A. [23]. They applied Cauchy's formula and, based on experimental values of water's refractive index collected from the literature across the spectral range 200 nm $\leq \lambda \leq$ 1000 nm and water temperature interval $0°$C $\leq t_w \leq 100°$C, they expressed the Cauchy coefficients as temperature-dependent functions. The authors consequently propose the following expression for $n(\lambda, t_w)$:

$$n(\lambda, t_w) = A(t_w) + \frac{B(t_w)}{\lambda^2} + \frac{C(t_w)}{\lambda^4} + \frac{D(t_w)}{\lambda^6}, \tag{27}$$

where

$$\begin{aligned}
A(t_w) &= 1.3208 - 1.2325\times10^{-5}t_w - 1.8674\times10^{-6}t_w^2 + 5.0233\times10^{-9}t_w^3,\\
B(t_w) &= 5208.2413 - 0.5179t_w - 2.284\times10^{-2}t_w^2 + 6.9608\times10^{-5}t_w^3,\\
C(t_w) &= -2.5551\times10^{8} - 18341.336t_w - 917.2319t_w^2 + 2.7729t_w^3,\\
D(t_w) &= 9.3495 + 1.7855\times10^{-3}t_w + 3.6733\times10^{-5}t_w^2 - 1.2932\times10^{-7}t_w^3.
\end{aligned}$$

3. Treatment of the problem within wave theory framework

The first rainbow theory that, by introducing wave effects such as interference and diffraction, achieved a finite maximum light intensity, was introduced by G. B. Airy [5] in 1838. A few years later, G. Mie [6] developed a comprehensive rainbow theory applying electromagnetic theory to light scattering by small particles. Although Mie theory is considered the exact theory of the rainbow, its predictions are very similar to those obtained from Airy's semiclassical approximation. On the one hand, the predictions from both theories are practically indistinguishable regarding the position of the intensity maxima. On the other hand, the high-frequency ripples predicted by Mie theory, superimposed on the Airy fringes, could only be observed under laboratory conditions involving monochromatic light scattered by a single droplet, not in a natural rainbow. [19,25,26]. Furthermore, easily calculable approximate mathematical expressions can be found in the literature that very faithfully represent the so-called Airy function, based on which the rainbow intensity is then calculated. In contrast, implementing Mie theory is considerably more cumbersome and time-consuming. Considering that we are not interested in exact light intensity values but rather in its behavior with certain parameters such as water temperature or drop size, and given that this article focuses on the primary rainbow, with phenomena like supernumerary arcs being beyond our current scope, we have chosen to work with Airy's theory.

To calculate the Airy function Ai for different values of its argument, X, we use the following expressions:

$$\begin{aligned}
Ai(-X) = A_0&\left(1 - \frac{X^3}{6} + \frac{X^6}{180}\right)\\
&+ A_1\left(-X + \frac{X^4}{12} - \frac{X^7}{504}\right),
\end{aligned} \tag{28}$$

with

$$\begin{aligned}
A_0 &= 0.355028053887817,\\
A_1 &= -0.258819403792807,
\end{aligned}$$

and

$$\begin{aligned}
Ai(-X) = \frac{1}{(\sqrt{\pi}X^{1/4})}&\left(\frac{5}{48X^{3/2}}\sin\left[\frac{2X^{3/2}}{3} - \frac{\pi}{4}\right]\right.\\
&\left.+\cos\left[\frac{2X^{3/2}}{3} - \frac{\pi}{4}\right]\right).
\end{aligned} \tag{29}$$

Eq. (28) is a Maclaurin series expansion, suitable to represent the Airy function for values of X close to 0, while Eq. (29) represents the first two terms of a Poincaré asymptotic expansion, appropriate to represent the Airy function for the remaining values of X. By joining both equations at $X = 1.76$, the Airy function is very well reproduced, at least for the values of X of interest in the context of this work. Both the Maclaurin series expansion and the Poincaré asymptotic expansion that approximately fits the Airy function can be found in the NIST Digital Library of Mathematical Functions [27, 28].

Regarding the argument of the Airy function, X, we use the expression in terms of λ, R, and n given by Nussenzveig [7], and employed by other authors [29, 30], namely:

$$X = (\gamma - \gamma_{m,MC}) \left(\frac{4\pi R}{3\lambda}\right)^{2/3} \frac{\left(n^2-1\right)^{1/2}}{\left(4-n^2\right)^{1/6}}, \qquad (30)$$

where $\gamma_{m,MC}$ is the angle γ of the minimum light deviation within the geometric optics framework. The light intensity of the rainbow as a function of the deviation angle γ will be given by

$$I(\gamma) = \mathcal{I}_0 F\, Ai^2(-X)\, (T_\perp + T_\parallel), \qquad (31)$$

where $T_\perp$ and $T_\parallel$ are given by Eqs. (11), being

$$F = \frac{2\pi R^2 \sin\alpha_{m,MC}}{\sin\gamma_{m,MC}} \left(\frac{32(n^2-1)^3\pi R}{81(4-n^2)\lambda}\right)^{1/3}. \qquad (32)$$

In this way,

$$\frac{d\sigma(\gamma)}{d\Omega} = F Ai^2(-X) \qquad (33)$$

represents an effective cross-section within Airy's theory framework (see [31, 32]), equivalent to the cross-section obtained in the geometric optics approach. Note that F is a function dependent on λ, R, and t_w through n.

4. Results and discussion. Geometrical optics, wave theory, and hybrid approach

We are interested not so much in the absolute values of the rainbow's light intensity but rather in its behavior with parameters such as water temperature, drop radius, wavelength, and light exit angle. In this regard, we are particularly interested in a potential comparison between geometric optics and wave-theory predictions. All our calculations were performed for the primary rainbow, so hereafter we omit the subscript m denoting the rainbow's order.

Although geometric optics predicts an infinite light intensity at the minimum deviation angle, we can estimate $I(\gamma)$ using Eq. (26). As explained in Sec. 2.4., applying Eq. (26) to calculate the light intensity of the rainbow requires first assuming a value for $\Delta\gamma$. For this purpose, we make the following considerations. We compute the angular width of the rainbow $(\gamma_b - \gamma_r)_{MC}$, that is, the angle between Descartes rays for the extreme wavelengths of the visible spectrum (*i.e.* blue and red). All observed rainbow colors are the result of light that emerges within this $\approx 2^\circ$ span. Since we distinguish colors, each wavelength covers only a fraction of this span. For a given wavelength, we can then write $\Delta\gamma = (\gamma_b - \gamma_r)_{MC}/N$, where N is a number greater than or equal to 2. $(\gamma_b - \gamma_r)_{MC}/2$ represents an upper bound for $\Delta\gamma$, since if at least two colors are not distinguished, there is no rainbow. This upper bound would imply a very poorly defined rainbow. As $\Delta\gamma$ decreases, there is less color mixing, and the rainbow becomes sharper. $N = 7$, for the seven traditional colors, might approximate a well-defined rainbow. Within the framework of geometric optics, we can do no more than carry out our calculations for different values of $\Delta\gamma$ in the interval $0 < \Delta\gamma \leq (\gamma_b - \gamma_r)_{MC}/2$, which we indeed did. However, we have taken advantage of the wave theory analysis of the rainbow and build a hybrid approach. Since wave theory concludes that the size of water drops determines how sharp the rainbow appears, $\Delta\gamma$ should depend on the drop radius. Given that we are interested in incorporating dependence on R (absent in the framework of pure geometric optics), we propose, first,

$$\Delta\gamma = \gamma_{h/2} - \gamma_{MW}, \qquad (34)$$

being γ_{MW} and $\gamma_{h/2}$ the values of γ for which Ai^2 reaches its maximum value and falls to half of this maximum, respectively. Henceforth, the subscript MW denotes *Maximum*, referring to peak intensity conditions, and *Wave*, indicating the wave theory framework we employ. We could observe that the approach given by Eq. (34) not only introduces dependence on R but also yields an intensity decay with γ comparable to the predictions of the Airy theory. After performing calculations across a broad range of values for parameters λ, R, and t_w, we observed that the geometric optic peak intensity consistently exceeded the predictions of Airy theory by ≈ 1.2. Consequently, we systematically determined the $\Delta\gamma$ values required to match the intensity predictions of both theories. From our analysis, we found that the appropriate values should be

$$\Delta\gamma = \left(\gamma_{h/2} - \gamma_{MW}\right) 1.44. \qquad (35)$$

Calculating $\Delta\gamma$ this way for a wide range of values of λ, R, and t_w, we verified that $\Delta\gamma$ depends strongly on R and moderately on λ, being completely negligible its dependence on t_w. For $R = 0.5$ mm and $\lambda = 500$ nm, for example, $\Delta\gamma = 0.28871^\circ$, which is approximately equal to $(\gamma_b - \gamma_r)_{MC}/6$. As R increases, $\Delta\gamma$ calculated using Eq. (35) decreases. Consequently, for $R = 2$ mm, $\Delta\gamma = 0.1162^\circ$ which is approximately equal to $(\gamma_b - \gamma_r)_{MC}/16$. In Fig. 5 we show $\Delta\gamma$, calculated using Eq. (35), as a function of R, for three λ values.

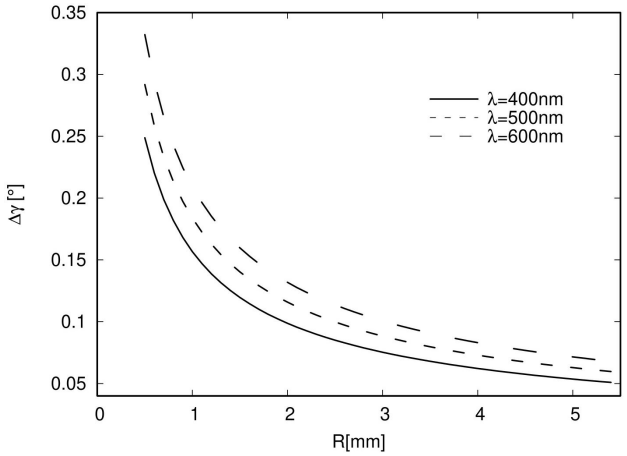

FIGURE 5. The interval $\Delta\gamma$ (see text) is displayed as a function of the water drop radius, R, for $\lambda = 400$ nm, $\lambda = 500$ nm and $\lambda = 600$ nm.

The curves shown in Fig. 5 can be fitted with the following function of R and λ:

$$\Delta\gamma[^\circ] = 18.677\lambda^{0.7515} \times \exp(-9.33R^{0.0735}) + 0.0076, \qquad (36)$$

with λ in nm and R in mm. Adopting $\Delta\gamma = (\gamma_{h/2} - \gamma_{MW})1.44$ as a function of R and λ, we calculate the corresponding intervals $\Delta\alpha$ by numerically solving Eq. (2). The $\Delta\alpha$ intervals thus calculated are shown plotted as a function of γ in the left panel of Fig. 6, for two different values of λ, two different values of R, and two different values of t_w. The symbols represent our calculations, while the curves joining them are fitting functions.

The first thing that stands out in Fig. 6 is that, for any set of parameter values, the value of $\Delta\alpha$ corresponding to the angle of minimum deviation is much larger than those corresponding to other exit angles. This allows for the usual interpretation, within the framework of geometric optics, of the existence of a maximum light intensity in the rainbow: all rays that strike the drop at an angle α with the radial direction within the large interval $\Delta\alpha$ emerge from it at an angle γ within a small range around the ray of minimum deviation. In other words, the densest clustering of rays exiting the drop after a single internal reflection occurs around γ_{MC}. The second thing clearly observed in the figure is that all values of $\Delta\alpha$, including those corresponding to the intensity maximum of the first-order rainbow, $\Delta\alpha_{MC}$, increase slightly with wavelength, in addition to undergoing the corresponding shift toward lower values of γ. However, as t_w increases, $\Delta\alpha$ does not vary, although a shift toward lower values of γ is observed. Regarding the dependence on R, from the left panel of Fig. 6 it is obvious that the variation of $\Delta\alpha$ with R, which arises from the introduction of a R-dependent value of $\Delta\gamma$, is much more pronounced than with other parameters. In addition to a marked decrease in the values of $\Delta\alpha$ as R increases, the rate of decline with γ increases. The latter means that, as R increases, each color is distributed over smaller intervals of γ values, which implies, in turn, a more defined rainbow.

On the other hand, if we want to extract information about the dependence of the rainbow's intensity on different parameters, analyzing the behavior of $\Delta\alpha$ alone is not enough. We must examine the behavior of the ratio $\Delta\alpha/\Delta\gamma$, to which the light intensity is proportional. We then turn to what we have plotted in the right panel of Fig. 6, namely, $\Delta\alpha/\Delta\gamma$ as a function of γ for the same two values of λ, R, and t_w as in the left panel. There, it can be observed that although $\Delta\alpha$ increases with λ and decreases with R, $\Delta\gamma$ grows and shrinks, respectively, much more strongly, so $\Delta\alpha/\Delta\gamma$ ends up being smaller for larger λ and larger for larger R. According to that, and since $\Delta\alpha/\Delta\gamma$ is the factor that primarily determines the rainbow's light intensity, as we explicitly state below, the rainbow would be more intense on its blue side than on its red side. This likely does not match our perception, given that there are factors we are not considering: the non-uniform distribution

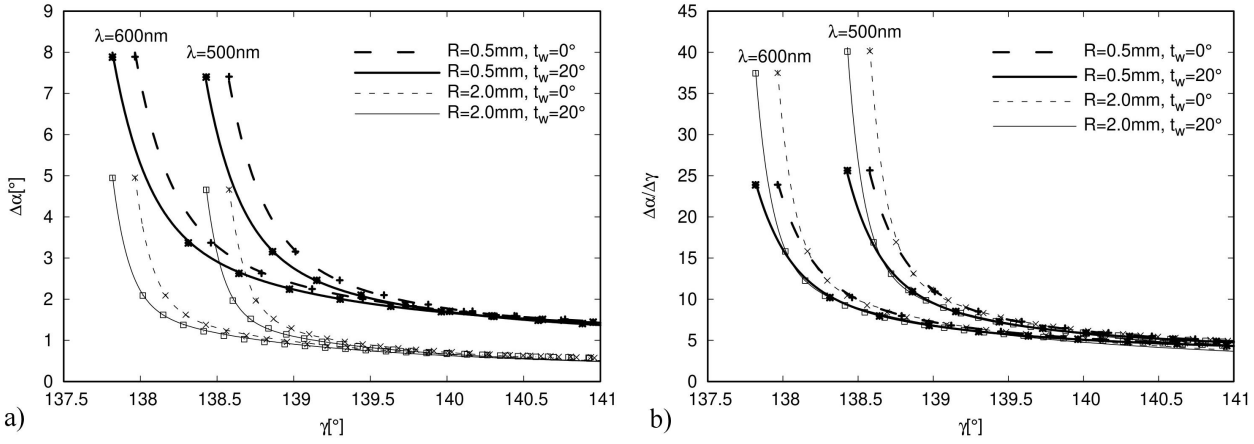

FIGURE 6. Interval $\Delta\alpha$ a) and $\Delta\alpha/\Delta\gamma$ b) as a function of the angle γ that the emerging ray makes with the incident ray direction (see text). In both panels the results obtained for $R = 0.5$ mm and $R = 2$ mm are plotted with thick and thin lines, respectively. Solid lines correspond to $t_w = 20^\circ$ C and dashed lines to $t_w = 0^\circ$ C.

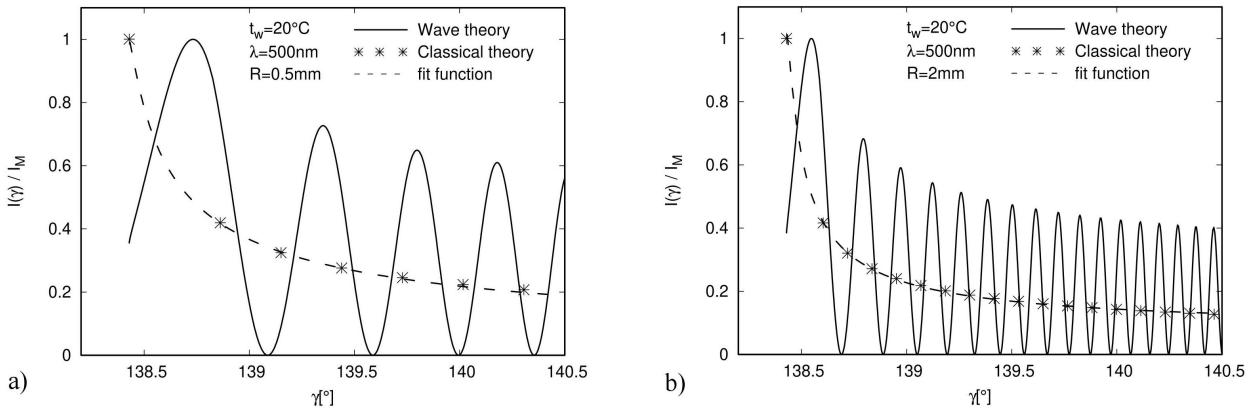

FIGURE 7. The luminous intensity of the first-order rainbow, normalized to its maximum value, is displayed as a function of the angle γ. Solid lines show the results obtained from Airy's theory, while symbols correspond to those derived from geometric optics, with dashed lines indicating fitting functions. The upper panel shows the results for $R = 0.5$ mm, and the lower panel for $R = 2$ mm. In both panels, $\lambda = 500$ nm and $t_w = 20^\circ$ C have been taken.

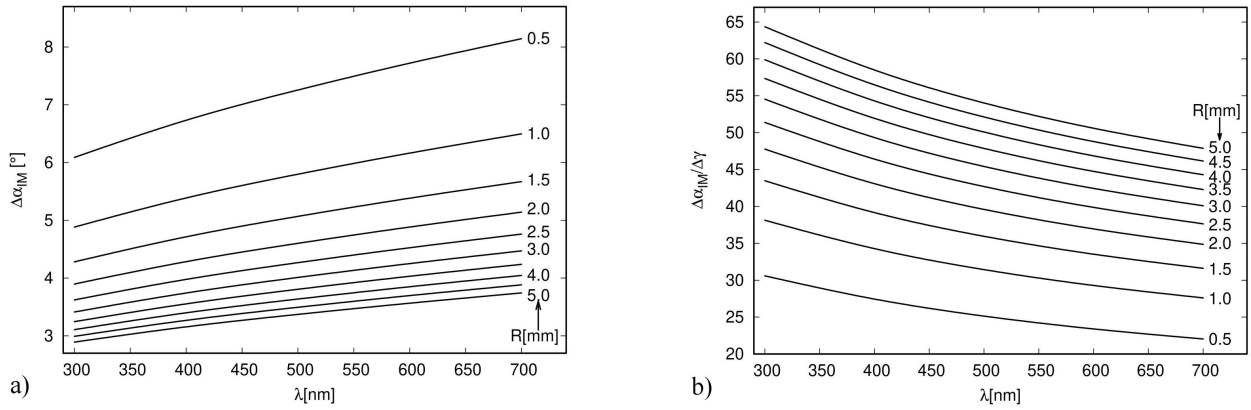

FIGURE 8. $\Delta\alpha_{MC}$, in the upper panel, and $\Delta\alpha_{MC}/\Delta\gamma$, in the lower panel, are displayed as functions of λ for different R values.

of sunlight intensity with wavelength, the greater attenuation that blue light undergoes when passing through the atmosphere between the drops and the observer's eyes, and the differential visual sensitivity of the human eye. As for the behavior of the rainbow's intensity with R, we reproduce the well-known result: larger drops produce more intense rainbows. Regarding the dependence on water temperature, we can conclude that this parameter does not affect the intensity of the rainbow, although it does influence its position. This is without prejudice to the potential influence that water temperature may have on other drop properties.

Once $\Delta\gamma$ and $\Delta\alpha$ are determined, we compute the light intensity using Eq. (26) for different values of λ, R, and t_w, which is shown in Fig. 7. In the upper panel we plot the light intensity as a function of γ obtained from Eq. (26), with $\Delta\alpha$ and $\Delta\gamma$ calculated as previously described, for $t_w = 20^\circ$ C, $\lambda = 500$ nm, and $R = 0.5$ mm. For the same values of t_w, λ, and R, we also plot the light intensity computed within Airy's theory framework using Eq. (31). The symbols in the figure represent discrete intensity values obtained from Eq. (26), and the dashed curve represents an exponential fitting function. Since our primary interest lies not in the absolute intensity values, but rather in their angular distribution, the intensities in Fig. 7 are normalized to their respective maximum values, I_M, in each case. The lower panel displays the same functions but calculated for $R = 2$ mm.

Figure 7 clearly reveals the well-known differences in the behavior of light intensity as a function of γ obtained within each theoretical framework. The wave treatment shows, on the one hand, the appearance of secondary maxima that account for the existence of supernumerary arcs. On the other hand, a shift of the primary maximum toward higher γ values is observed compared to the results obtained from geometric optics, a shift that furthermore shows a strong dependence on the drop radius. By introducing a $\Delta\gamma$ dependent on R (and on λ), which only appears as a multiplicative factor in the purely classical treatment, we achieve a drop size dependence of $I(\gamma)$ similar to that observed in the wave treatment. Thus, the decrease in intensity with γ is more pronounced for larger values of R in both cases, as can be seen in the figure.

Once the behavior of the luminous intensity with the exit angle has been analyzed, we aim to highlight the behavior of the first-order rainbow peak with the light's wavelength, the water temperature, and the drop size, separately. In Fig. 8

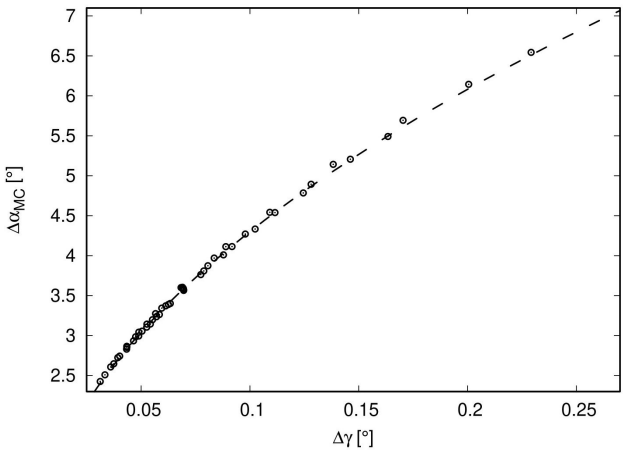

FIGURE 9. $\Delta\alpha_{MC}$ is desplayed as a function of $\Delta\gamma$.

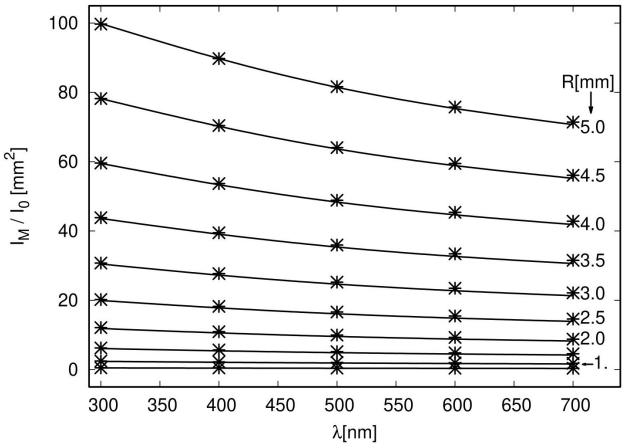

FIGURE 10. First-order rainbow peak intensity, normalized to incident light, as a function of λ. Classical (solid lines) and Airy theory (symbols) results are compared for different R values.

$\Delta\alpha_{MC}$ a) and $\Delta\alpha_{MC}/\Delta\gamma$ b) are plotted, both as functions of λ for different values of R. It is apparent that while $\Delta\alpha_{MC}$ grows as λ grows and decreases as R grows, the behavior of $\Delta\alpha_{MC}/\Delta\gamma$ is the other way around with both variables. $\Delta\alpha_{MC}$ can be written as a function of λ as

$$\Delta\alpha_{MC}[^\circ] = C_1\lambda^2 + C_2\lambda + C_3, \tag{37}$$

being C_1, C_2, and C_3, the following functions on R:

$$\begin{aligned} C_1 &= -0.00000411576R^{-0.258637} + 0.0000014, \\ C_2 &= 0.009587556R^{-0.268863} - 0.0026829, \\ C_3 &= 2.808R^{-0.330559} + 0.313407, \end{aligned} \tag{38}$$

with λ in nm and R in mm.

Alternatively, $\Delta\alpha_{MC}$ can be written as a function of $\Delta\gamma$ as shown in Fig. 9. In this figure, the symbols stand for our calculations carried on for 300 nm $\leq \lambda \leq$ 700 nm, 0° C $\leq t_w \leq 50^\circ$ C, and 0.5 mm $\leq R \leq$ 5 mm, being the dashed line the best fit curve given by

$$\Delta\alpha_{MC} = 13.6\sqrt{\Delta\gamma}, \tag{39}$$

with both $\Delta\alpha$ and $\Delta\gamma$ expressed in $^\circ$. Using either Eq. (37) or Eq. (39) to calculate $\Delta\alpha_{MC}$ avoids the numerical solution of Eq. (2). Note that neither $\Delta\alpha_{MC}$ nor $\Delta\alpha_{MC}/\Delta\gamma$ depend on t_w.

With $\Delta\gamma$ and $\Delta\alpha_{MC}$ calculated as explained above, the maximum intensity with respect to the incident intensity is obtained as follows:

$$\frac{I_{MC}}{\mathcal{I}_0} = R^2 \frac{\sin\alpha_{MC}\cos\alpha_{MC}}{\sin\gamma_{MC}} \left(T_\perp + T_\parallel\right)_{MC} \frac{\Delta\alpha_{MC}}{\Delta\gamma}. \tag{40}$$

We were able to verify that for all values of α_{MC} obtained from 300 nm $\leq \lambda \leq$ 700 nm and 0° C $\leq t_w \leq 50^\circ$ C,

$$\frac{\sin\alpha_{MC}\cos\alpha_{MC}}{\sin\gamma_{MC}} \left(T_\perp + T_\parallel\right)_{MC} \approx 0.06. \tag{41}$$

Note that, just like $\Delta\alpha_{MC}/\Delta\gamma$, this is a dimensionless quantity. Therefore, $I_{MC}/\mathcal{I}_0$ has the units of R^2.

Taking into account also that $\Delta\alpha_{MC}/\Delta\gamma$ can be calculated as a function of λ and R, either by dividing Eq. (37) by Eq. (36) or, more simply, by dividing Eq. (39) by Eq. (36), the maximum intensity with respect to the incident intensity can be calculated as a function of λ and R as follows:

$$\frac{I_{MC}}{\mathcal{I}_0} = \frac{0.816R^2}{\left(18.677\lambda^{0.7515}\exp(-9.33R^{0.0735}) + 0.0076\right)^{1/2}}, \tag{42}$$

which is temperature-independent. In Fig. 10 the maximum intensity, relative to the incident intensity, of the first-order rainbow is plotted as a function of λ, for different R values. Solid lines show geometric optics predictions obtained from Eq. (40), while symbols denote results from Airy theory. The plot clearly shows that the results derived from both theories are nearly identical. It is also evident that, within the framework of both theories, all rainbow colors are more intense if the drops are larger. A decrease in peak intensity with wavelength is also observed, with the decrease being sharper for larger drops under both theoretical approaches. This dependence of rainbow intensity on droplet size and wavelength, which causes the droplet size to influence both the rainbow's global brightness and the relative intensity of its constituent colors, was described in early works by authors like [15].

Although the intensity does not depend on the water temperature, the position of the peak is indeed influenced by this parameter. To show the effect of temperature on peak intensity, in Fig. 11 we plot the corresponding values of α_M and γ_M as functions of t_w. α_{MW} and γ_{MW}, calculated using Airy's theory, are plotted as functions of t_w for $R = 0.5$ mm, in panels a) and d), and for $R = 2$ mm, in panels b) and e). α_{MC} and γ_{MC}, calculated using geometric optics, are plotted as functions of t_w in panels c) and f). Panels a)-f) show results for two representative wavelengths, $\lambda = 500$ nm and $\lambda = 600$ nm. It is worth mentioning that, although we calculated the values γ_{MW} in the Airy theory framework using

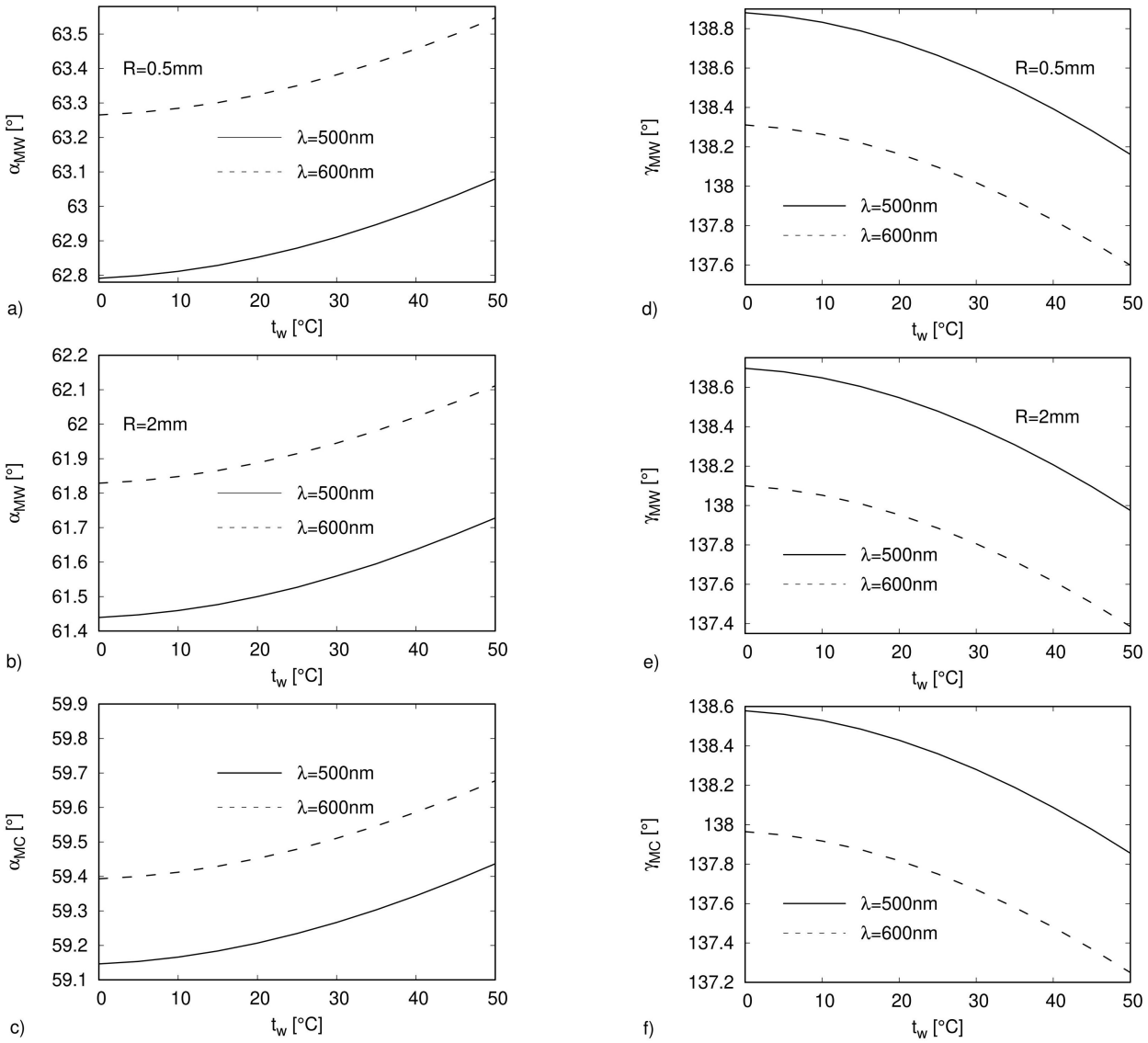

FIGURE 11. Plotted as functions of water temperature are: the incidence angle corresponding to the rainbow's intensity maximum in panels a), b), and c); the emergence angle corresponding to the rainbow's intensity maximum in panels d), e), and f). The upper panels show α_{MW} and γ_{MW} obtained from Airy's theory for $R = 0.5$ mm, the middle panels show α_{MW} and γ_{MW} obtained from Airy's theory for $R = 2$ mm, and the lower panels show α_{MC} and γ_{MC} obtained from classical theory. α_{MW}, γ_{MW}, α_{MC}, and γ_{MC} are displayed for $\lambda = 500$ nm, with solid lines, and $\lambda = 600$ nm with dashed lines.

a numerical code based on the full expression of Eq. (31), these values could also have been derived from the argument of the Airy function given by Eq. (30). Considering that the first maximum of the Airy function occurs at $X = -1.01879$, similar γ_{MW} values can be obtained, since the $T_\perp + T_\parallel$ factor introduces a negligible correction to the peak locations.

In Fig. 11 we can see that, within both theoretical frameworks and for any value of R, while the value of α corresponding to the intensity peak increases with both temperature and wavelength, the corresponding value of γ decreases with these parameters. This means that for a given wavelength and drop size, as the water temperature rises, the rainbow peak occurs at a lower γ angle, which in turn corresponds to a higher α angle. Since a larger α angle implies a larger impact parameter b, this indicates that as t_w increases, the light that contributes the most to the rainbow formation enters the drop closer to its edge. For fixed λ and R, the variation in α_{MC} and α_{MW} with t_w reaches $\approx 0.3^\circ$ as t_w increases from 0° C to 50° C, while the change in γ_{MC} and γ_{MW} reaches $\approx 0.7^\circ$ in the same temperature range.

Meanwhile, Fig. 12 depicts the values of α_M and γ_M as functions of R, for different values of λ and t_w. As shown in this figure, when R is varied from 0.2 mm to 6 mm, the change in γ_{MC} and γ_{MW} remains within a few tenths of a degree, while the variation in α_{MC} and α_{MW} is considerably more pronounced. The horizontal lines represent the results obtained within the geometric optics framework, which are independent of R, for the adopted values of t_w and λ.

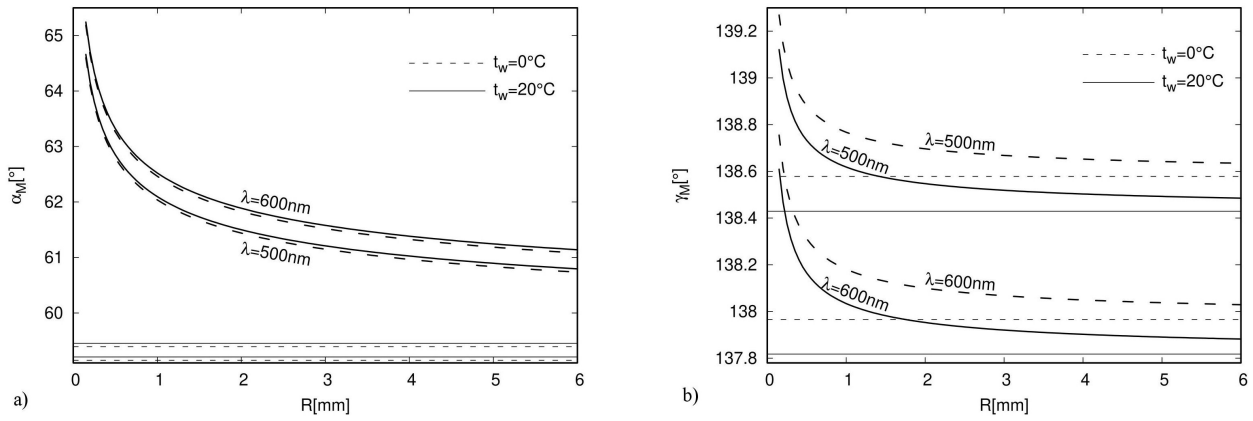

FIGURE 12. α_M and γ_M are displayed as functions of R for two different λ values and two different R values. Curved lines correspond to Airy theory results, while straight lines indicate geometric optics predictions.

We compared our results with those presented by Van Beeck in Ref. [19], taking advantage of the fact that his work includes Figs. 4.11, 4.12, 5.4, and 5.5, which show the angular positions of the Airy fringe maxima as functions of droplet size and water temperature. We confirmed that the position of the first Airy fringe maximum we found deviates from that reported by Van Beeck [19] by approximately one hundredth of a degree. This discrepancy arises from the use of different expressions for the refractive index of water. While we employed the function of λ and T proposed by A. N. Bashkatov and E. A. Genina [23], Van Beeck used an expression provided by Thormählen *et al*. [33], which depends on λ, T, and atmospheric pressure (P). We verified that the refractive index values we obtained are approximately one thousandth higher than those reported by Van Beeck [19] for $P = 1$ atm.

From our calculations, we derived the following expressions representing α_{MC}, γ_{MC}, α_{MW} and γ_{MW} as functions of t_w, λ and R:

$$\alpha_{MC} = 0.000091893\, t_w^2 + 0.0013079\, t_w - 0.00000358256\, \lambda^2 + 0.00639156\, \lambda + 56.8408, \tag{43}$$

$$\gamma_{MC} = -0.000232835\, t_w^2 - 0.00324744\, t_w + 0.00000851481\, \lambda^2 - 0.0154691\, \lambda + 144.201, \tag{44}$$

$$\alpha_{MW} = 0.000091893\, t_w^2 + 0.0013079\, t_w - 0.00000358256\, \lambda^2 + 0.00639156\, \lambda + 56.8408 + 36.6017 \left(\frac{\lambda}{R}\right)^{0.333898}, \tag{45}$$

$$\gamma_{MW} = -0.000232835\, t_w^2 - 0.00324744\, t_w + 0.00000851481\, \lambda^2 - 0.0154691\lambda + 144.201 + 40.1912 \left(\frac{\lambda}{R}\right)^{0.709909}, \tag{46}$$

with λ and R in nm and t_w in °C. From these expressions it follows that for large values of R the results obtained using Airy's theory approach the solution found within the framework of geometric optics. This is clearly evidenced in Fig. 12, where the curves obtained using Airy's theory asymptotically approach the horizontal lines representing the results derived from geometric optics.

5. Summary and conclusions

In this article we have explored two aspects of the rainbow that, to our knowledge, have not been previously addressed beyond their conceptual consideration.

On one hand, we have overcome the obstacle that, in the classical treatment, arises from the singularity that the differential cross-section exhibits at the minimum deflection angle by discretizing the problem. In this way, we have calculated the outgoing light not for different values of the exit angle γ, but rather for different intervals of γ. The crux of the matter then lies in adopting an appropriate discretization. First, we established $\Delta\gamma = (\gamma_b - \gamma_r)_{MC}/2$ as the maximum bound for the interval of γ values within which light of a given wavelength is distributed. To incorporate the dependence on R we later have adopted $\Delta\gamma = (\gamma_{h/2} - \gamma_{MW})1.44$. This ensures that the light intensity distribution with respect to the exit angle depends on R (and, of course, on λ) in a manner analogous to that of Ai^2. Using this methodology, we have first calculated $\Delta\gamma$ for different sets of values of variables λ, R, and t_w. Second, for different γ values, we have computed the contributing intervals $\Delta\alpha$ corresponding to the calculated $\Delta\gamma$. Finally, we have determined the light intensity for various values of λ, R, and t_w. Regarding the absolute values of the light intensity, we have verified that choosing $\Delta\gamma = (\gamma_{h/2} - \gamma_{MW})1.44$, which is a function of λ and R, it results $I_{MC} \approx I_{MW}$, for any value of λ, R, and t_w.

On the other hand, we have introduced the dependence of the rainbow light intensity on water temperature. Given that this dependence arises from the relationship between the re-

fractive index and the temperature of the water, an expression for n as a function of both t_w and λ has been adopted from the literature. We confirmed that the dependence of light intensity on t_w, if any, is entirely negligible, while the variation in the angular width of the rainbow as t_w changes is barely perceptible. However, we observed that water temperature does alter the distribution of I with respect to γ and, consequently, the position of the intensity maxima.

According to theoretical models and in situ measurements, raindrop temperature is typically a few tenths of a degree below the wet-bulb temperature and rarely exceeds $35°$C [34–36]. Nevertheless, we varied t_w from $0°$C to $50°$C to account for exceptional scenarios where the drop temperatures might surpass this value. Such cases could occur in natural settings, such as rainfall with high ambient temperatures and humidity [37] or near geysers, or in artificial environments such as industrial or laboratory conditions.

The following results focus on how the first-order rainbow's peak position varies with water temperature and drop radius:

1) For a given wavelength, the minimum deviation angles in both theories, γ_{MC} and γ_{MW}, decrease as the temperature increases, while the impact-related angles, α_{MC} and α_{MW}, increase with t_w. While α_M exhibits a modest shift of $\approx 0.3°$ as t_w increases from $0°$C to $50°$C, γ_M shows a more pronounced shift of $\approx 0.7°$. The temperature-induced shift in γ_M suggests a measurable change in the observed rainbow angle, though small, it could be relevant for precision optics modeling. Both classical and wave theories predict the same trends with temperature.

2) Regarding size dependence, the γ_M angles show variation of $\approx 0.5°$ throughout the drop size range, while the α_M angles exhibit, in the same range, a much stronger variation of $\approx 4°$. The stronger R-dependence on α indicates significant changes in light entry conditions. Both parameters show a strong dependence on R for small drops ($R < 0.5$ mm), being much more stable across drop sizes for $R \geq 1$ mm. Then, the wave theory results deviate from geometric optics, particularly for smaller drops.

We have illustrated our results in numerous figures and expressed them as functions of the different variables whenever possible. We particularly highlight Eqs. (42) and (46), simple expressions that allow us to calculate both the intensity and the position of the first-order rainbow maximum as functions of λ, R, and t_w. The classical terms show explicit dependence on t_w and λ, while the wave theory introduces additional R-dependence. For large drops ($R \gg \lambda$) the wave theory results converge to classical solutions as wave effects become negligible, confirming the correspondence principle between wave and geometric optics.

We aim to explore the specific dependence of the rainbow pattern on atmospheric conditions, which, in turn, determine the properties of water drops. Lv and coworkers [22] found that for cooling droplets, the volume-averaged temperature measured by rainbow refractometry is higher than the drop surface temperature, whereas the opposite is true for heating droplets. In the context of a natural rainbow, it is clear that we are dealing with the latter scenario (heating drops). Although Lv and colleagues [22] did not work with water, they found entirely similar results for the three different liquids they experimented with. According to these authors, when the initial temperature of a heating drop is approximately ≈ 20 K lower than the ambient temperature, the deviation between the surface temperature and the volume-averaged temperature obtained via rainbow refractometry is less than $1°$K. It is only when the ambient temperature is hundreds of degrees higher than the drop initial temperature that temperatures deduced by each technique could differ by approximately $10°$K, which is not a realistic scenario in nature. Therefore, we conclude that it is appropriate to extract raindrop characteristics by analyzing the natural rainbow pattern and to subsequently infer atmospheric conditions.

1. C. A. Paola, A. Cruzado, and F. M. Carrasco Galleguillos, Light refraction in the earth's atmosphere I. Inferior mirages: analytic solution of ray paths, *Rev. Mex. Fis.* **68** 4 (2022) 041301 1. https://doi.org/10.31349/RevMexFis.68.041301
2. A. Cruzado, A. Cesanelli and C. A. Paola, Light refraction in the earth's atmosphere II. Inferior mirages: regions for images and objects observation, *Rev. Mex. Fis.* **69** 6 (2023) 061303 1. https://doi.org/10.31349/RevMexFis.69.061303
3. C. A. Paola, A. Cruzado and A. Cesanelli, Light refraction in the earth's atmosphere III. Inferior mirages: images locus, *Rev. Mex. Fis.* **70** 3 (2024) 031301 1. https://doi.org/10.31349/RevMexFis.70.031301
4. T. Young, The Bakerian Lecture. Experiments and calculations relative to physical optics, *Phil. Trans. R. Soc.* **94** (1804) 1. https://doi.org/10.1098/rstl.1804.0001
5. G. B. Airy, On the intensity of light in the neighbourhood of a caustic, *Trans. Cambridge Philos. Soc.* **6** (1838) 379. ID: 209973084.
6. G. Mie, Beiträge zur Optik trüber Medien, speziell kolloidaler Metallösungen, *Ann. Phys.* **330** 3 (1908) 377. https://doi.org/10.1002/andp.19083300302
7. H. M. Nussenzveig, High Frequency Scattering by a Transparent Sphere. II. Theory of the Rainbow and the Glory, *J. Math. Phys.* **10** (1969) 125. https://doi.org/10.1063/1.1664747
8. H.M. Nussenzveig, The theory of the rainbow, *Scientific American*, **236** (1977) 116. https://doi.org/10.1038/scientificamerican0477-116
9. H.M. Nussenzveig, Diffraction Effects in Semiclassical Scattering (University Press, Cambridge, 1992) pp 101-116. https://doi.org/10.1017/CBO9780511599903

10. J. D. Walker, Multiple rainbows from single drops of water and other liquids, *Am. J. Phys.* **44** (1976) 421. https://doi.org/10.1119/1.10172
11. S. D. Mobbs, Theory of the Rainbow, *J. Opt. Soc. Am.* **69** (1979) 1089. https://doi.org/10.1364/JOSA.69.001089.
12. G. Casini, A. Covello, The rainbow in the drop, *Am. J. Phys.* **80** 11 (2012) 1027. https://doi.org/10.1119/1.4732530.
13. R. A. R. Tricker, Introduction to meteorological optics (American Elsevier Pub. Co., 1970) pp. 42-69, pp. 169-190, pp. 210-229.
14. R. Greenler, Rainbows, halos and glories (Society of Photo-Optical Instrumentation Engineers, Bellingham, Washington USA, 2020). https://doi.org/10.1117/3.2573017
15. M. G. J. Minnaert, Light and colours in the outdoors (Springer New York, NY., 1993) pp 185-258. https://doi.org/10.1007/978-1-4612-2722-9
16. N. Roth, K. Anders, and A. Frohn, Simultaneous measurement of temperature and size of droplets in the micrometer range, *J. Laser Appl.* **2** (1990) 37. https://doi.org/10.2351/1.4745251
17. N. Roth, K. Anders, and A. Frohn, Refractive-index measurements for the correction of particle sizing methods *Appl. Opt.* **30** (1991) 4960. https://doi.org/10.1364/AO.30.004960
18. J. P. A. J. Van Beeck and M. L. Riethmuller, M. L., Simultaneous determination of temperature and size of droplets from the rainbow using Airy theory. Developments in Laser Techniques and Applications to Fluid Mechanics: Proceedings of the 7th International Symposium Lisbon, Portugal, 11-14 July, 1994 (Berlin, Heidelberg: Springer Berlin Heidelberg, 1996) pp. 330-339.
19. J. P. A. J. Van Beeck, Rainbow phenomena: development of a laser-based, non-intrusive technique for measuring droplet size, temperature and velocity. [Phd Thesis 2 (Research NOT TU/e / Graduation TU/e), Applied Physics and Science Education]. Technische Universiteit Eindhoven, The Netherlands (1997). https://doi.org/10.6100/IR493789
20. S. Saengkaew, Development of novel global rainbow technique for characterizing spray generated by ultrasonic nozzle. Chulalongkorn University Theses and Dissertations (Chula ETD). 65622 (2005). https://digital.car.chula.ac.th/chulaetd/65622
21. Chanisa Kanjanasakul, Analysis of the optical properties of droplets of different fluids in high-pressure environments by rainbow optical diagnostic. Physics [physics]. Normandie Université (2017). https://theses.hal.science/tel-01791028v1/file/CK.pdf
22. Lv. Qimeng, Wu. Yingchun, and Wu. Xuecheng, Surface temperature measurement of cooling and heating droplets by rainbow refractometry, *Appl. Opt.* **61** (2022) 7455. https://doi.org/10.1364/AO.470123
23. A. N. Bashkatov, E. A. Genina, Water refractive index in dependence on temperature and wavelength: a simple approximation, *Proc. SPIE* **5068** (2003) 393. https://doi.org/10.1117/12.518857
24. E. Kendir, S. Yaltkaya, Effect of temperature and wavelength on the refractive index of water: a fiber-optic sensor application, *Indian J. Phys.* **96** (2022) 1247. https://doi.org/10.1007/s12648-021-02064-7
25. R. L. Lee Jr., Mie theory, Airy theory, and the natural rainbow, *Appl. Opt.* **37** (1998) 1506. https://doi.org/10.1364/AO.37.001506
26. P. Laven, Simulation of rainbows, coronas, and glories by use of Mie theory, *Appl. Opt.* **42** (2003) 436. https://doi.org/10.1364/AO.42.000436
27. F. W. J. Olver, Airy and Related Functions, National Institute of Standards and Technology (NITS), Digital Library of Mathematical Functions, Chapter 9 (2010). https://dlmf.nist.gov/9.4.
28. F. W. J. Olver, Airy and Related Functions, National Institute of Standards and Technology (NITS), Digital Library of Mathematical Functions, Chapter 9 (2010). https://dlmf.nist.gov/9.7.E9.
29. M.V. Berry and S. Klein, Diffraction near fake caustics, *Eur. J. Phys.* **18** (1997) 303. https://dx.doi.org/10.1088/0143-0807/18/4/011.
30. M. V. Berry, Nature's optics and our understanding of light, *Contemp. Phys.* **56** (2015) 2. https://dx.doi.org/10.1080/00107514.2015.971625.
31. J. A. Adam, The mathematical physics of rainbows and glories, *Phys. Rep.* **356** (2002) 229. https://doi.org/10.1016/S0370-1573(01)00076-X.
32. J.D. Jackson, From Alexander of Aphrodisias to Young and Airy, *Phys. Rep.* **320** (1999) 27. https://doi.org/10.1016/S0370-1573(99)00088-5.
33. I. Thormählen, J. Straub, and U. Grigull, Refractive Index of Water and Its Dependence on Wavelength, Temperature, and Density, *J. Phys. Chem. Ref. Data* **14** (1985) 933. https://doi.org/10.1063/1.555743.
34. R. Gosnell, C. W. Fairall, and P. J. Webster. The sensible heat of rainfall in the tropical ocean. *Journal of Geophysical Research: Oceans* **100** C9 18437-18442. https://doi.org/10.1029/95JC01833.
35. C. Raymond, T. Matthews, and R. M. Horton, The emergence of heat and humidity too severe for human tolerance, *Science Advance* **6** (2020) 1. https://doi.org/10.1126/sciadv.aaw1838.
36. S. P. Anderson, A. Hinton, and R. A. Weller, Moored observations of precipitation temperature, *Journal of Atmospheric and Oceanic Technology* **15** (1998) 979. https://doi.org/10.1175/1520-0426(1998)015⟨0979:MOOPT⟩2.0.CO;2.
37. J. Master. Hottest rain on record? Rain falls at 109°F in Saudi Arabia, *Wunderground Category 6* (2012). https://www.wunderground.com/blog/JeffMasters/hottest-rain-on-record-rain-falls-at-109f-in-saudi-arabia.html.